Control of individual electron-spin pairs in an electron-spin bath

Bartling, H. P.; Demetriou, N.; Zutt, N. C.F.; Kwiatkowski, D.; Degen, M. J.; Loenen, S. J.H.; Bradley, C. E.; Markham, M.; Twitchen, D. J.; Taminiau, T. H.

DOI
10.1103/PhysRevResearch.7.013333

Publication date
2025

Document Version
Final published version

Published in
Physical Review Research

Control of individual electron-spin pairs in an electron-spin bath

H. P. Bartling,[1,2,*] N. Demetriou,[1,2,*] N. C. F. Zutt,[1,2] D. Kwiatkowski,[1,2] M. J. Degen,[1,2] S. J. H. Loenen,[1,2] C. E. Bradley,[1,2] M. Markham,[3] D. J. Twitchen,[3] and T. H. Taminiau[1,2,†]

[1]*QuTech, Delft University of Technology, PO Box 5046, 2600 GA Delft, The Netherlands*

[2]*Kavli Institute of Nanoscience Delft, Delft University of Technology, PO Box 5046, 2600 GA Delft, The Netherlands*

[3]*Element Six, Fermi Avenue, Harwell Oxford, Didcot, Oxfordshire OX11 0QR, United Kingdom*

(Received 16 November 2023; accepted 19 February 2025; published 31 March 2025)

The decoherence of a central electron spin due to the dynamics of a coupled electron-spin bath is a core problem in solid-state spin physics. Ensemble experiments have studied the central spin coherence in detail, but such experiments average out the underlying quantum dynamics of the bath. Here, we show the coherent back-action of an individual NV center on an electron-spin bath and use it to detect, prepare, and control the dynamics of a pair of bath spins. We image the NV-pair system with subnanometer resolution and reveal a long dephasing time [$T_2^* = 44(9)$ ms] for a qubit encoded in the electron-spin pair. Our experiment reveals the microscopic quantum dynamics that underlie the central spin decoherence and provides new opportunities for controlling and sensing interacting spin systems.

DOI: 10.1103/PhysRevResearch.7.013333

Solid-state spins provide a versatile platform for quantum science and technology, as well as for studying the fundamentals of spin coherence. A canonical case is the central spin problem: a single, central spin coupled to a surrounding bath of interacting spins [1–10]. A common approach to protect the central spin from decoherence due to the bath spins is to use echo or decoupling sequences. Under such echo sequences, the system undergoes complex quantum dynamics that depend on the microscopic bath configuration and on the back-action of the central spin on the interacting spin bath [1–10].

For an electron spin in a nuclear-spin bath, the large magnetic moment of the electron spin strongly affects the nuclear-spin bath evolution. The resulting back-action creates rich dynamics under echo sequences on the central spin [11–13] and has enabled the control of tens of individual nuclear spins [14,15], pairs of coupled nuclear spins [12,13,16,17], and collective excitations [18,19] in the spin bath.

For an electron spin in an electron-spin bath, the effect of back-action is more subtle. All couplings are of similar strength and they are typically weak compared to the energy splittings. The resulting central spin decoherence has been investigated in detail in ensemble experiments [3,5,9,10,20], which have been described by semiclassical models, as well as by fully quantum models using approximate numerical methods [3,5,8–10,21]. In such ensemble experiments, the underlying microscopic quantum dynamics are averaged out. Single-spin experiments have been performed with NV centers in diamond [2,4,22–28]. However, the coherence under echo sequences [29] could be satisfactorily described by an effective magnetic field noise (an Ornstein-Uhlenbeck process) [1,4,7,9]. In this classical model of the spin bath, the back-action of the central spin is neglected and the central limit theorem is used to approximate the bath as Gaussian, forgoing the microscopic quantum dynamics.

Here, we show that the microscopic flip-flop dynamics in an electron-spin bath can be experimentally accessed and controlled using echo sequences on a central spin. Compared to previous work, we observe a single central electron spin, rather than an ensemble average, and use time-resolved correlations and real-time logic to prepare and observe specific configurations of the bath, rather than averaging over all states. We demonstrate strong back-action of a central electron spin on the dynamics of an individual spin pair in the bath, and use this coherent interaction to detect, image, and control the spin pair. We show that the spin pair can be used to encode a controllable qubit with long coherence times [$T_2^* = 44(9)$ ms], due to a combination of a decoherence-free subspace and a clock transition. Our results directly access the microscopic quantum dynamics that underlie the central spin decoherence and provide new opportunities for controlling interacting spin systems.

We investigate a single nitrogen-vacancy (NV) center in diamond surrounded by a bath of P1 centers (nitrogen defects) at a temperature of 3.3 K (Fig. 1). The P1 concentration is ∼75 ppb, and the estimated ^{13}C concentration is 0.01% [24,30]. The NV electron spin acts as the central spin and is initialized optically and read out using spin-selective optical excitation (637 nm) [16,24].

*These authors contributed equally to this work.
†Contact author: T.H.Taminiau@TUDelft.nl

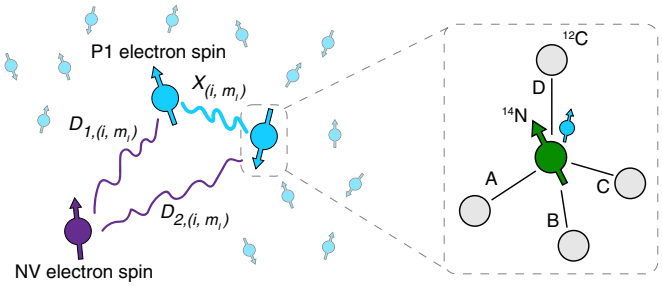

FIG. 1. Schematic of the spin system. We detect and control the dynamics of a pair of P1 electron spins in a P1 bath through the back-action from an NV center. The inset shows the lattice structure of a P1 center in diamond with the ^{14}N nuclear spin (spin states $m_I \in \{-1, 0, +1\}$) and four axes ($i \in \{A, B, C, D\}$) for the Jahn-Teller distortion, which spontaneously breaks the tetrahedral symmetry by shifting the nitrogen atom along one of the four N-C bonds. $X_{(i,m_I)}$ is the effective coupling between the P1 electron spins and $D_{(i,m_I)}$ are the effective couplings with the NV center electron spin.

The P1 centers have multiple internal, dynamic degrees of freedom: the electron spin-1/2, four different Jahn-Teller (JT) axes, and a spin-1 ^{14}N nuclear spin (Fig. 1). The combined ^{14}N and JT state is stable without illumination (time scale of 40 s), but fluctuates under laser excitation [24]. The P1 Hamiltonian for the JT axis $i \in \{A, B, C, D\}$ is [31]

$$H_{P1,i} = \gamma_e \mathbf{B} \cdot \mathbf{J} + \gamma_n \mathbf{B} \cdot \mathbf{I} + \mathbf{J} \cdot \mathbf{A}_i \cdot \mathbf{I} + \mathbf{I} \cdot \mathbf{P}_i \cdot \mathbf{I}, \qquad (1)$$

where γ_e (γ_n) is the electron (nitrogen) gyromagnetic ratio and $\mathbf{J}$ ($\mathbf{I}$) is the electron spin-1/2 (^{14}N nuclear spin-1) operator vector. $\mathbf{A}_i$ ($\mathbf{P}_i$) is the hyperfine (quadrupole) tensor where the subscript i indicates the Jahn-Teller axis [24,32]. We apply a few-degree misaligned magnetic field with respect to the NV axis $\mathbf{B} = [2.43(2), 1.42(3), 45.552(3)]$ G to lift the degeneracy for the different JT axes [33].

Since the NV-P1 dipolar coupling can be approximated as $\hat{S}_z \hat{J}_z$ [34], echo sequences on the NV electron spin primarily probe the energy-conserving flip-flop dynamics of the P1 bath due to the dipolar P1-P1 couplings. Whether flip-flops between two P1 centers are allowed depends on their electron and ^{14}N spin states, on their JT axes, and on the local magnetic field due to the NV, ^{13}C spins, and other nearby P1 centers. Therefore, the dynamics are complex, depend strongly on the specific microscopic configuration, and change over time.

We probe and prepare specific bath configurations by performing time-resolved experiments through repeated NV measurement sequences. This is made possible by the long lifetime of the JT axis and ^{14}N spin at cryogenic temperatures and by a low-intensity resonant readout of the NV spin that only weakly perturbs the P1 center states [24]. Previous room-temperature experiments with high-power off-resonant lasers rapidly average over all P1 states [2,4,22,35,36].

We apply dynamical decoupling sequences consisting of π pulses with variable spacing 2τ [Fig. 2(a)], which sense the bath dynamics around a frequency of $1/(4\tau)$. We repeatedly apply the sequence, bin m outcomes together, and analyze the signal and correlations over time. Figure 2(b) shows a time trace, revealing discrete jumps in the NV coherence. A

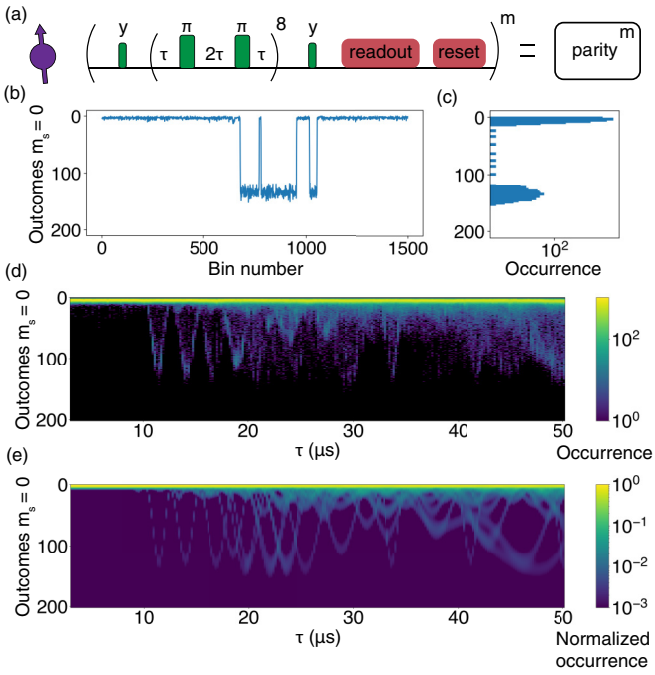

FIG. 2. Repetitive dynamical decoupling spectroscopy of a P1 center bath. (a) Experimental sequence. (b) Time trace for $\tau = 14.2\,\mu$s and bin-size $m = 200$. (c) Histogram of a three-minute-long time trace for $\tau = 14.2\,\mu$s and $m = 200$. We rarely observe a high number of $m_s = 0$ occurrences (~1.3%). Due to limited observations, the fraction of ~1.3% is likely not a precise measure of the probability of occurrence. (d) Repetitive dynamical decoupling spectroscopy of a P1 bath surrounding an NV center. We apply the sequence shown in (a) for $m = 200$. (e) Simulation of the repetitive dynamical decoupling spectroscopy in (d) for a system of one NV center and two P1 centers with the positions as obtained in Fig. 4. Note that in (e) we assume equal occurrence of all ^{14}N and JT states, and we do not take into account potential ^{14}N and JT state changes during the $m = 200$ sequence repetitions. For more details, see [33]. Further deviations between (d) and (e) may be caused by the presence of other, weaker P1 spin pairs. Note that single ^{13}C spins would shift the entire yellow band down due to the lack of internal degrees of freedom and can therefore not explain deviations between (d) and (e).

longer-time histogram [Fig. 2(c)] reveals that the signal is a rare occurrence, which would be easily lost in the noise in a time-averaged measurement.

We create a map of the bath dynamics by collecting histograms as a function of the interpulse delay τ [Fig. 2(d)]. The result shows distinct resonances for various values of τ, which we attribute to two coupled P1 centers in the bath switching to different electron-spin, JT, and ^{14}N configurations. For each configuration, the P1 spin pair flip-flops with a characteristic frequency, which is resonant with the sensing sequence for a particular τ.

To analyze the results, we consider a single pair of P1 centers. For a large magnetic field, the electron- and nuclear-spin basis states are proper P1 eigenstates. Energy-conserving electron-spin flip-flops are then allowed when the two P1 centers have identical JT and ^{14}N states. As exploited extensively for nuclear-spin pairs [12,13,16,17], the dynamics can then be

described by a pseudo-spin in the antiparallel spin subspace ($|\Uparrow\rangle = |\uparrow\downarrow\rangle$ and $|\Downarrow\rangle = |\downarrow\uparrow\rangle$).

The pseudo-spin Hamiltonian [12,13,16,17], including the effect of the NV center, is

$$H_{(i,m_l)} = X_{(i,m_l)}\hat{S}_x + m_s Z_{(i,m_l)}\hat{S}_z, \tag{2}$$

where $\hat{S}_x, \hat{S}_z$ are spin-1/2 operators, $X_{(i,m_l)}$ is the effective spin-pair coupling, $Z_{(i,m_l)}$ is a detuning due to the different couplings to the central NV spin, and m_s is the NV spin projection. For large magnetic fields, there are 12 such Hamiltonians (four JT axes and three ^{14}N states), all with equal values for X and Z [33]. For the field applied here, which is of the order of the hyperfine interaction ($\gamma_e B \sim A_\parallel, A_\perp$), the electron- and nuclear-spin states mix. Therefore, flip-flop interactions involving the nuclear spin are possible, and $X_{(i,m_l)}$ and $Z_{(i,m_l)}$ depend on the JT and spin states involved. We use the high-field spin labels for simplicity, but take the modified eigenstates and additional flip-flop interactions into account in our analysis.

Next, we demonstrate the initialization, control, and measurement of the P1-pair state. From the mathematical equivalence with previous work [6,11,16], it follows that the Hamiltonian in Eq. (2) yields an effective $\hat{S}_z^{\mathrm{NV}}\hat{S}_z$ interaction under a resonant dynamical decoupling sequence with $2\tau = \pi/\omega_r$ with $\omega_r = \sqrt{X^2 + (Z/2)^2}$. The NV electron spin thus picks up a positive or negative phase depending on the state of the P1-pair pseudo-spin [16]. No phase is picked up when the pair is in the parallel subspace ($|\uparrow\uparrow\rangle$, $|\downarrow\downarrow\rangle$), nor for any combination of JT and ^{14}N states that do not cause flip-flop dynamics at the resonant frequency ω_r.

To initialize the P1 pair in a particular JT and ^{14}N state and in the antiparallel subspace, we apply repeated "parity" readouts [Fig. 2(a)], and put a threshold on the obtained counts. We implement real-time logic to speed-up the initialization procedure: during the 50 parity readouts we keep track of the obtained counts and we restart the procedure if heralding successful preparation becomes unlikely [33]. This yields a $\sim$10$\times$ speed-up of the experiments and is essential for enabling the presented measurements.

To initialize the spin pair, we apply repeated "spin" readouts [Fig. 3(a)]. Subsequent spin measurements are time-matched to account for the evolution of the spin pair during one spin readout, similar to previous experiments with repeated measurements on precessing nuclear spins [16,33,37].

By choosing a different interpulse delay τ, we can address different JT and ^{14}N states. We can thus measure the dependence of the electron-electron couplings (X and Z) on the JT and ^{14}N states by performing Ramsey-type experiments using different values of τ. Figure 3(b) shows the Ramsey-type measurements with the NV electron in $m_s = 0$. The $m_s = -1$ case can be found in [33]. In these measurements, the spin pair is initialized in $|\uparrow\downarrow\rangle$. During the free evolution time t, the pair periodically evolves following $|\uparrow\downarrow\rangle \Leftrightarrow |\downarrow\uparrow\rangle$ (flip-flop). Finally, the probability to observe the initial state $|\uparrow\downarrow\rangle$ is measured.

To investigate the spin-pair coherence, we measure the dephasing time for $\tau = 14.0\,\mu$s [Fig. 3(c)]. We find $T_2^* = 44(9)$ ms, among the longest reported for solid-state electron-spin qubits [38]. Compared to the single P1 electron-spin

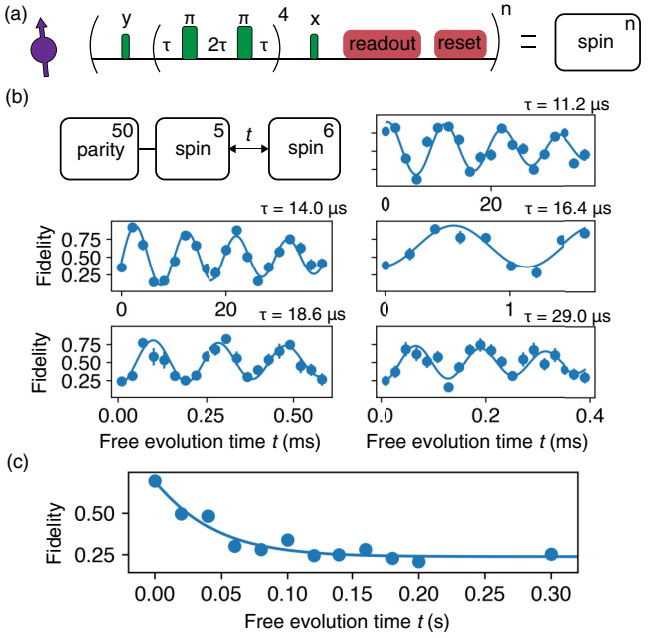

FIG. 3. Ramsey-type measurements and coherence of the P1 spin pair. (a) Experimental sequence to measure the pseudo-spin state ($\{|\uparrow\downarrow\rangle\}$ vs $\{|\downarrow\uparrow\rangle\}$) [33]. (b) Ramsey-type measurements with the NV electron spin in $m_s = 0$ during free evolution, for five interpulse delays τ chosen at signal dips in Fig. 2(d). We apply 50 parity readouts and herald initialization for $\geqslant 15$ counts. We then apply five spin readouts, which herald initialization in $|\uparrow\downarrow\rangle$ ($|\downarrow\uparrow\rangle$) for $\geqslant 1$ ($= 0$) counts. We use six spin readouts to measure the final spin-pair state, assigning $\geqslant 2$ ($\leqslant 1$) counts to $|\uparrow\downarrow\rangle$ ($|\downarrow\uparrow\rangle$). The contrast is limited by the pseudo-spin dephasing during the spin initialization and readout [33]. (c) Bloch vector length measurement of the spin pair at $\tau = 14.0\,\mu$s, obtaining $T_2^* = 44(9)$ ms. The data is not corrected for the readout infidelity.

coherence $T_2^* = 50(3)\,\mu$s [24], this is a three-order-of-magnitude improvement in the same nuclear- and electron-spin bath. Two mechanisms contribute to this long dephasing time. First, the antiparallel spin-pair states from a decoherence-free subspace: they are insensitive to the partially correlated noise from the P1 bath [16]. And second, the spin pair forms a clock transition due to the P1-P1 coupling [16,33].

Next, we determine what JT and ^{14}N states are associated to the signals for the different interpulse delays τ. Due to the electron-nuclear hyperfine interaction and misaligned, finite magnetic field, the electron-spin transition frequency is different for each JT and ^{14}N state. After initializing the electron-spin pair in $\frac{1}{2}|\uparrow\downarrow\rangle\langle\uparrow\downarrow| + \frac{1}{2}|\downarrow\uparrow\rangle\langle\downarrow\uparrow|$ for an unknown JT and ^{14}N state, we apply a radio-frequency (RF) pulse that—when resonant—can flip the spin pair to the parallel subspace resulting in a change in signal on the NV center [Fig. 4(a)]. The RF frequencies at which electron-spin flips occur, give information about the JT and ^{14}N state associated to that τ [33].

Figure 4(a) shows the data for both $\tau = 11.2\,\mu$s and $\tau = 14.0\,\mu$s. In order to map the obtained frequencies to the JT and ^{14}N state, we simulate the experiment for each JT and ^{14}N configuration [33]. From this, we obtain a set of

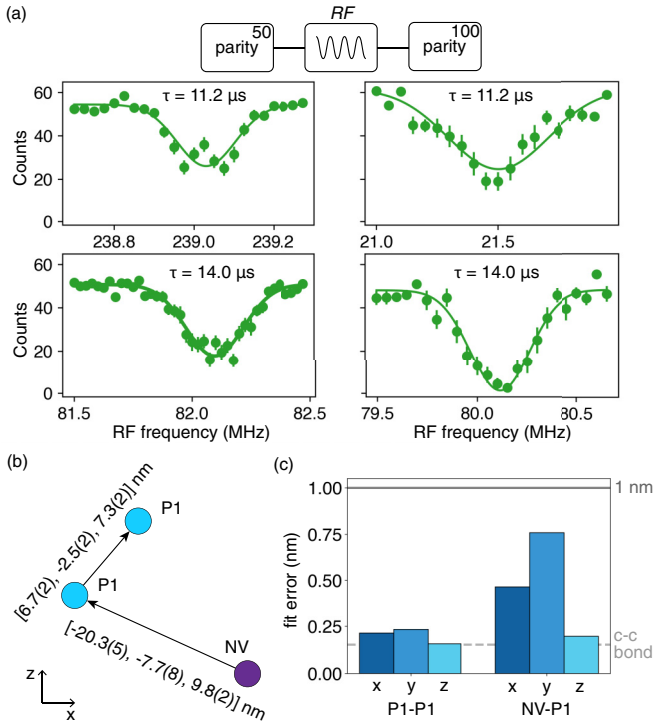

FIG. 4. RF driving and imaging of the P1 electron-spin pair. (a) (Top) Experimental sequence. The spin pair is initialized in $\frac{1}{2}|\uparrow\downarrow\rangle\langle\uparrow\downarrow| + \frac{1}{2}|\downarrow\uparrow\rangle\langle\downarrow\uparrow|$, after which an RF pulse of varying frequency can flip the spin pair to the parallel subspace [33]. (Bottom) Spectra for $\tau = 11.2\,\mu$s (top) and $\tau = 14.0\,\mu$s (bottom). A reduction in counts gives information about the JT and ^{14}N state probed for that τ. (b) Fitted positions (up to inversion symmetry) of the two P1 centers (blue) with respect to the NV center (purple). (c) Fit errors for the P1-P1 and NV-P1 positions.

possible Jahn-Teller axis and ^{14}N spin state assignments [33]. We perform the same analysis for $\tau = 16.8\,\mu$s, $\tau = 18.6\,\mu$s, and $\tau = 29.0\,\mu$s [33].

While the JT axis can be directly assigned, the ^{14}N spin-state assignment is more complicated. Due to the electron-nitrogen spin mixing, flip-flops can occur that involve both the electron and nitrogen spin, creating additional possible transitions [33]. Next, we resolve this ambiguity by determining for which of the possible state assignments a consistent spatial structure of the system can be found.

The spin-pair couplings obtained in Fig. 3(b) combined with the associated JT and ^{14}N states allow us to image the P1 electron-spin pair [39]. We fit the five measured P1-P1 couplings to different spatial configurations of the P1 pair. Multiple ^{14}N spin-state assignments are possible for three out of five measured couplings [33]. We resolve this by considering all possible assignments in the fit. We benchmark the fitting algorithm on ten randomly generated P1 pairs [33], after which we apply it to the measured couplings. The result yields the relative position of the two P1 centers with an uncertainty close to the diamond bond length [Figs. 4(b) and 4(c)], as well as the JT and ^{14}N states associated to the τ resonances [33].

We find the position of the NV center, using a similar fitting algorithm [33]. In Degen *et al.* [24] double-resonance sequences were used to measure the dipolar couplings of the NV center to the two P1 centers. We fix the obtained P1-P1 relative position and fit to the NV-P1 couplings (up to inversion symmetry). The result is shown in Figs. 4(b) and 4(c).

A coherent interaction between the NV and the P1-pair requires the interaction time (set by $1/Z$) to be small compared to the spin-pair dephasing time (T_2^*) and the NV electron-spin coherence time under decoupling (T_2). A key element in our experiment is that the large number of different internal P1 states cause energy differences that prevent flip-flop dynamics in the bath. This extends the NV spin coherence and facilitates selective addressing of individual spin pairs, at the cost of a lower success probability for finding a given pair in the desired configuration. The full microscopic dynamics including the P1 and ^{13}C nuclear-spin bath are complex. Predicting the typical number of P1 spin pairs that would be observed for randomly drawn NV centers (i.e., bath instances) likely requires detailed numerical simulation using, for example, correlated cluster expansion (CCE), which we do not pursue here.

In conclusion, we experimentally demonstrated the detection, imaging, and control of an electron-spin pair in a spin bath through the back-action from a central spin. These results experimentally access the underlying microscopic quantum dynamics which are central to theoretical methods, such as correlated cluster expansion (CCE), that have been widely used to understand time- and ensemble-averaged measurements [3,5,6,8,10,21]. The long dephasing times indicate electron-spin pairs based on P1 centers or other defects [25,26,40,41] might be interesting qubits. While the added complexity from the P1 internal states limits its use as a qubit, this could be partly overcome by applying a large, aligned magnetic field [33]. Lastly, the presented methods could contribute to efforts toward atomic-scale magnetic resonance imaging of complex spin samples outside of the diamond by directly detecting and imaging spin pairs [15,42].

We thank V. V. Dobrovitski and M. H. Abobeih for discussions. This work was supported by the Netherlands Organisation for Scientific Research (NWO/OCW) through a Vidi grant, as part of the Frontiers of Nanoscience (NanoFront) programme and through the project QuTech Phase II funding: "Quantum Technology for Computing and Communication" (Project No. 601.QT.001). This project has received funding from the European Research Council (ERC) under the European Union's Horizon 2020 research and innovation programme (Grant Agreement No. 852410). This project (QIA) has received funding from the European Union's Horizon 2020 research and innovation programme under Grant Agreement No. 820445.

DATA AVAILABILITY

The fitting algorithms were performed on the DelftBlue supercomputer at Delft University of Technology [43]. Data underlying the study are available upon request.

[1] J. R. Klauder and P. W. Anderson, Spectral diffusion decay in spin resonance experiments, Phys. Rev. **125**, 912 (1962).
[2] R. Hanson, V. V. Dobrovitski, A. E. Feiguin, O. Gywat, and D. D. Awschalom, Coherent dynamics of a single spin interacting with an adjustable spin bath, Science **320**, 352 (2008).
[3] W. M. Witzel, M. S. Carroll, A. Morello, L. Cywiński, and S. Das Sarma, Electron spin decoherence in isotope-enriched silicon, Phys. Rev. Lett. **105**, 187602 (2010).
[4] G. de Lange, Z. H. Wang, D. Ristè, V. V. Dobrovitski, and R. Hanson, Universal dynamical decoupling of a single solid-state spin from a spin bath, Science **330**, 60 (2010).
[5] W. M. Witzel, M. S. Carroll, L. Cywiński, and S. Das Sarma, Quantum decoherence of the central spin in a sparse system of dipolar coupled spins, Phys. Rev. B **86**, 035452 (2012).
[6] N. Zhao, S. W. Ho, and R. B. Liu, Decoherence and dynamical decoupling control of nitrogen vacancy center electron spins in nuclear spin baths, Phys. Rev. B **85**, 115303 (2012).
[7] W. M. Witzel, K. Young, and S. Das Sarma, Converting a real quantum spin bath to an effective classical noise acting on a central spin, Phys. Rev. B **90**, 115431 (2014).
[8] H. Seo, A. L. Falk, P. V. Klimov, K. C. Miao, G. Galli, and D. D. Awschalom, Quantum decoherence dynamics of divacancy spins in silicon carbide, Nat. Commun. **7**, 1 (2016).
[9] E. Bauch, S. Singh, J. Lee, C. A. Hart, J. M. Schloss, M. J. Turner, J. F. Barry, L. M. Pham, N. Bar-Gill, S. F. Yelin, and R. L. Walsworth, Decoherence of ensembles of nitrogen-vacancy centers in diamond, Phys. Rev. B **102**, 134210 (2020).
[10] H. Park, J. Lee, S. Han, S. Oh, and H. Seo, Decoherence of nitrogen-vacancy spin ensembles in a nitrogen electron-nuclear spin bath in diamond, npj Quantum Inf. **8**, 95 (2022).
[11] T. H. Taminiau, J. Cramer, T. van der Sar, V. V. Dobrovitski, and R. Hanson, Universal control and error correction in multi-qubit spin registers in diamond, Nat. Nanotechnol. **9**, 171 (2014).
[12] F. Shi, X. Kong, P. Wang, F. Kong, N. Zhao, R.-B. Liu, and J. Du, Sensing and atomic-scale structure analysis of single nuclear-spin clusters in diamond, Nat. Phys. **10**, 21 (2014).
[13] M. H. Abobeih, J. Cramer, M. A. Bakker, N. Kalb, M. Markham, D. J. Twitchen, and T. H. Taminiau, One-second coherence for a single electron spin coupled to a multi-qubit nuclear-spin environment, Nat. Commun. **9**, 2552 (2018).
[14] C. E. Bradley, J. Randall, M. H. Abobeih, R. C. Berrevoets, M. J. Degen, M. A. Bakker, M. Markham, D. J. Twitchen, and T. H. Taminiau, A ten-qubit solid-state spin register with quantum memory up to one minute, Phys. Rev. X **9**, 031045 (2019).
[15] G. L. van de Stolpe, D. P. Kwiatkowski, C. E. Bradley, J. Randall, M. H. Abobeih, S. A. Breitweiser, L. C. Bassett, M. Markham, D. J. Twitchen, and T. H. Taminiau, Mapping a 50-spin-qubit network through correlated sensing, Nat. Commun. **15**, 2006 (2024).
[16] H. P. Bartling, M. H. Abobeih, B. Pingault, M. J. Degen, S. J. H. Loenen, C. E. Bradley, J. Randall, M. Markham, D. J. Twitchen, and T. H. Taminiau, Entanglement of spin-pair qubits with intrinsic dephasing times exceeding a minute, Phys. Rev. X **12**, 011048 (2022).
[17] N. Zhao, J. L. Hu, S. W. Ho, J. T. Wan, and R. B. Liu, Atomic-scale magnetometry of distant nuclear spin clusters via nitrogen-vacancy spin in diamond, Nat. Nanotechnol. **6**, 242 (2011).
[18] D. M. Jackson, D. A. Gangloff, J. H. Bodey, L. Zaporski, C. Bachorz, E. Clarke, M. Hugues, C. Le Gall, and M. Atatüre, Quantum sensing of a coherent single spin excitation in a nuclear ensemble, Nat. Phys. **17**, 585 (2021).
[19] A. Ruskuc, C.-J. Wu, J. Rochman, J. Choi, and A. Faraon, Nuclear spin-wave quantum register for a solid-state qubit, Nature (London) **602**, 408 (2022).
[20] A. M. Tyryshkin, S. Tojo, J. J. L. Morton, H. Riemann, N. V. Abrosimov, P. Becker, H.-J. Pohl, T. Schenkel, M. L. W. Thewalt, K. M. Itoh, and S. A. Lyon, Electron spin coherence exceeding seconds in high-purity silicon, Nat. Mater. **11**, 143 (2012).
[21] M. Ye, H. Seo, and G. Galli, Spin coherence in two-dimensional materials, npj Comput. Mater. **5**, 44 (2019).
[22] G. de Lange, T. Van Der Sar, M. Blok, Z. H. Wang, V. Dobrovitski, and R. Hanson, Controlling the quantum dynamics of a mesoscopic spin bath in diamond, Sci. Rep. **2**, 382 (2012).
[23] H. S. Knowles, D. M. Kara, and M. Atatüre, Observing bulk diamond spin coherence in high-purity nanodiamonds, Nat. Mater. **13**, 21 (2014).
[24] M. J. Degen, S. J. H. Loenen, H. P. Bartling, C. E. Bradley, A. L. Meinsma, M. Markham, D. J. Twitchen, and T. H. Taminiau, Entanglement of dark electron-nuclear spin defects in diamond, Nat. Commun. **12**, 3470 (2021).
[25] E. L. Rosenfeld, L. M. Pham, M. D. Lukin, and R. L. Walsworth, Sensing coherent dynamics of electronic spin clusters in solids, Phys. Rev. Lett. **120**, 243604 (2018).
[26] A. Cooper, W. K. C. Sun, J.-C. Jaskula, and P. Cappellaro, Identification and control of electron-nuclear spin defects in diamond, Phys. Rev. Lett. **124**, 083602 (2020).
[27] H. S. Knowles, D. M. Kara, and M. Atatüre, Demonstration of a coherent electronic spin cluster in diamond, Phys. Rev. Lett. **117**, 100802 (2016).
[28] D. Yudilevich, R. Stöhr, A. Denisenko, and A. Finkler, Mapping single electron spins with magnetic tomography, Phys. Rev. Appl. **18**, 054016 (2022).
[29] Note that double-resonance sequences, which manipulate multiple spins, have been exploited to detect single electron spins [24,26–28], including P1 centers, as well as signatures of flip-flop dynamics in spin clusters [25].
[30] C. E. Bradley, S. W. de Bone, P. F. W. Möller, S. Baier, M. J. Degen, S. J. H. Loenen, H. P. Bartling, M. Markham, D. J. Twitchen, R. Hanson, D. Elkouss, and T. H. Taminiau, Robust quantum-network memory based on spin qubits in isotopically engineered diamond, npj Quantum Inf. **8**, 122 (2022).
[31] W. V. Smith, P. P. Sorokin, I. L. Gelles, and G. J. Lasher, Electron-spin resonance of nitrogen donors in diamond, Phys. Rev. **115**, 1546 (1959).
[32] R. J. Cook and D. H. Whiffen, Electron nuclear double resonance study of a nitrogen centre in diamond, Proc. R. Soc. Lond. A **295**, 99 (1966).
[33] See Supplemental Material at http://link.aps.org/supplemental/10.1103/PhysRevResearch.7.013333 for more details of the system Hamiltonian, RF driving, imaging, Ramsey experiments, dephasing mechanisms, and spin and parity readout.

[34] In contrast, for a nuclear-spin bath the $\hat{S}_z\hat{J}_x$ terms are typically important [6,11].

[35] C. A. J. Ammerlaan and E. A. Burgemeister, Reorientation of nitrogen in type-I*b* diamond by thermal excitation and tunneling, Phys. Rev. Lett. **47**, 954 (1981).

[36] F. J. Heremans, G. D. Fuchs, C. F. Wang, R. Hanson, and D. D. Awschalom, Generation and transport of photoexcited electrons in single-crystal diamond, Appl. Phys. Lett. **94**, 152102 (2009).

[37] K. S. Cujia, J. M. Boss, K. Herb, J. Zopes, and C. L. Degen, Tracking the precession of single nuclear spins by weak measurements, Nature (London) **571**, 230 (2019).

[38] K. C. Miao, J. P. Blanton, C. P. Anderson, A. Bourassa, A. L. Crook, G. Wolfowicz, H. Abe, T. Ohshima, and D. D. Awschalom, Universal coherence protection in a solid-state spin qubit, Science **369**, 1493 (2020).

[39] As an alternative to using the internal degrees of freedom of the P1 center, one could sweep the external magnetic field angle [26,28].

[40] F. Shi, Q. Zhang, B. Naydenov, F. Jelezko, J. Du, F. Reinhard, and J. Wrachtrup, Quantum logic readout and cooling of a single dark electron spin, Phys. Rev. B **87**, 195414 (2013).

[41] T. Yamamoto, C. Müller, L. P. McGuinness, T. Teraji, B. Naydenov, S. Onoda, T. Ohshima, J. Wrachtrup, F. Jelezko, and J. Isoya, Strongly coupled diamond spin qubits by molecular nitrogen implantation, Phys. Rev. B **88**, 201201(R) (2013).

[42] E. Janitz, K. Herb, L. A. Völker, W. S. Huxter, C. L. Degen, and J. M. Abendroth, Diamond surface engineering for molecular sensing with nitrogen–vacancy centers, J. Mater. Chem. C **10**, 13533 (2022).

[43] Delft High Performance Computing Centre (DHPC), Delft-Blue Supercomputer (Phase 1), https://www.tudelft.nl/dhpc/ark:/44463/DelftBluePhase1.